Virtual Friction for Oscillation Damping and Inertia Sharing from Multi-Terminal VSC-HVDC Grids

Alberto Rodríguez-Cabero*, Javier Roldán-Pérez*, Milan Prodanovic*, Jon Are Suul†, Salvatore D'Arco†
*Electrical Systems Unit, IMDEA Energy Institute, Madrid, Spain. †SINTEF Energy Research, Trondheim, Norway.
{alberto.rodriguez, javier.roldan, milan.prodanovic}@imdea.org, {jon.a.suul, salvatore.darco}@sintef.no

***Abstract*—This paper proposes a control scheme for multi-terminal HVDC (MTDC) interconnections that introduces an effect equivalent to a mechanical coupling between asynchronous ac networks providing damping of frequency oscillations and frequency support. From the control systems perspective this virtual mechanical coupling is equivalent to a mechanical friction interconnecting the ac networks (modelled as equivalent rotating masses). Also, the control system provides an inertia sharing effect. These two properties can be used to effectively damp frequency oscillations, and provide frequency and inertia support to any ac network connected simultaneously. It is shown that the controller can effectively attenuate poorly damped oscillations that are observed at the MTDC terminals. The dynamic properties of the proposed controller are analysed and its impact of the stability of the three ac networks is evaluated by using a simplified model. The controller was validated by using detailed simulations.**

I. Introduction

The expected massive integration of renewable energy sources (RES) to power networks can lead to a stressed transmission system and additional network reinforcements may be necessary to resolve the congestions. High-voltage direct current (HVDC) transmission introduces several advantages over conventional high-voltage alternating current (HVAC), such as: increased efficiency (since large amounts of power can be transmitted over long distances), power transmission over mid-long distances by using insulated cables and interconnection of asynchronous power networks [1, 2]. Moreover, HVDC transmission systems have become a preferred solution over HVAC when it comes to dealing with the variability of RESs and the integration of massive amounts of wind energy through submarine cables.

A well known problem in power systems at the transmission level are low-frequency electro-mechanical oscillations, which are largely defined by the dynamic properties of synchronous generators, speed governors, excitation systems and the power system topology [3]. It is clear that the main purpose of HVDC transmission systems must be related to energy transmission over long distances. However, since the early practical applications of HVDC technology in the transmission system, many other features for grid stability enhancement and power oscillation damping (POD) methods have also been investigated for HVDC interconnections [4, 5]. Recent research works have been focused on the potential contribution of VSC-HVDC links to the grid stability enhancement in power networks with high penetration of RES [6]. In this sense, most research works have followed two main approaches. On the one hand, some authors have proposed control strategies based on the virtual synchronous machine (VSM) concept or inertia emulation in order to compensate low-inertia power systems [7]. On the other hand, other authors have presented solutions based on communication systems between the HVDC terminals. The latter provide good results, but most control methods have issues regarding their practical implementation: the use of high-bandwidth communications and its impact on the system reliability, dc-link voltage regulation, control complexity, etc.

In order to compensate for the inevitable reduced equivalent system inertia of future networks, some authors have proposed specific control strategies for VSC-HVDC interconnections based on the VSM concept and inertia emulation [8–10]. This control scheme has been well received by system operators since power systems are inherently designed to operate with synchronous generators. Moreover, if their control parameters are properly set, such converters can contribute to the power system stabilisation. However, the conventional control structure used for VSC-HVDC links imply a cascade control configuration based on an inner power/VSM controller and an outer dc-voltage controller. Unfortunately, this control scheme implies that the time constant of the dc-voltage control has to be in the same time scale (or slower) than that of the VSM. However, this situation leads to an undesired slow regulation of the dc-link voltage, thus threatening the system stability.

Other authors have highlighted the potential of VSC-HVDC transmission links to damp oscillations in emerging power system configurations. For example, Zeni *et al.* [11] proposed a guideline for control parameter tuning in order to damp the oscillations in VSC-HVDC links connected to offshore wind-farms. Moreover, the authors evaluated the impact of practical implementation effects like communication delays or ramp-rate limitations, which are commonly neglected in the literature. In [12], a supplementary controller based on heuristic dynamic programming (HDP) was introduced to damp inter-area modes. The method provides accurate results, but it is computationally intensive. The selection of the control parameters requires an intensive pre-training process under

The work of IMDEA Energy Institute received financial support from Community of Madrid, through the research project PROMINT-CM, Ref: P2018/EMT4366. The work of SINTEF Energy Research was supported by the project HVDC Inertia Provision (HVDC Pro), financed by the ENERGIX program of the Research Council of Norway (project number 268053/E20) and the industry partners; Statnett, Equinor, RTE and ELIA.

This is the accepted version of an article published in 2020 IEEE Energy Conversion Congress and Exposition - ECCE
http://dx.doi.org/10.1109/ECCE44975.2020.9235831

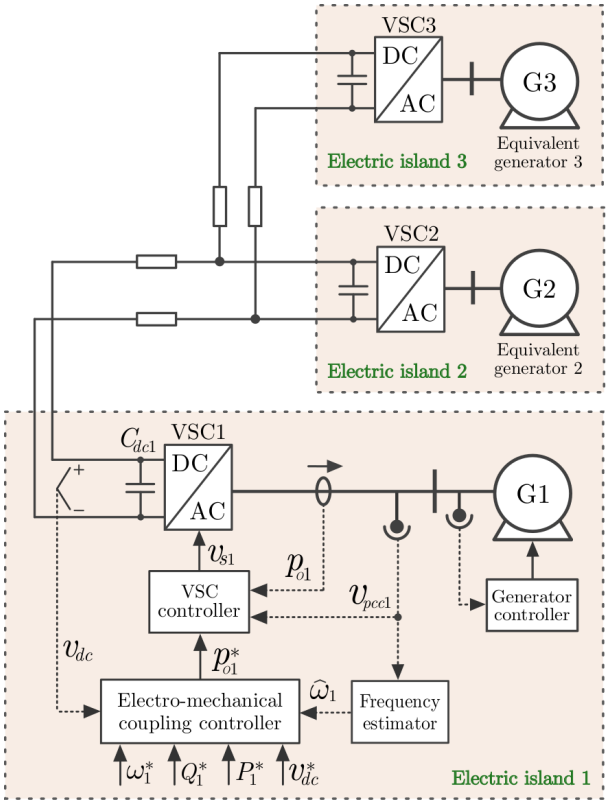

Fig. 1. Electrical diagram of the MTDC grid showing details of VSC1 control system.

different operation conditions and disturbances. Other authors focused on control strategies for POD by using wide area measurement signals (WAMS) [13, 14]. These control strategies showed satisfactory performance, but the requirement for fast communication links increases the system complexity and reduces reliability [15].

This paper proposes a control scheme for multi-terminal VSC-HVDC grids that introduces a virtual electro-mechanical coupling between three ac power systems. The proposed controller is based on the general concepts introduced in [16], where two interconnected power systems are modelled by their equivalent swing equation models. The mathematical modelling and the equivalent effect of the proposed controller are derived, and the POD capability is analytically evaluated by using a simplified model. Finally, the performance of the proposed controller is validated by using numerical simulations.

II. System Overview and Modelling

A. System Description

Fig. 1 shows the electrical system diagram of the multi-terminal VSC-HVDC grid studied in this paper. It consist of three VSCs (VSC1 to VSC3) connected to three independent ac grids that are modelled as equivalent synchronous generators (G1 to G3). The MTDC terminals have current/power controllers to control the active and reactive power delivered to the ac grids. The proposed controller is implemented on a secondary level and generates the active power references (p^*_o) for the inner controllers. The voltage of the point of common coupling (PCC) of MTDC terminals is v_{pcc}, i_o is the grid-side current, v_s is the VSC output voltage, and v_{dc} is the dc-capacitor voltage. The terminal number (1 to 3) is marked in the subscript of variables (e.g. i_{o1}). Each VSC has a dc capacitor called C_{dc} (e.g. C_{dc1}) and the total capacitance at the MTDC grid is $C'_{dc} = C_{dc1} + C_{dc2} + C_{dc3}$.

B. Synchronous Generator Modelling

Each terminal is connected to an ac network that has been modelled as an equivalent synchronous generator. The linearised shaft equation of the n-equivalent generator can be written as follows [17]:

$$2H_{g,n}\frac{d\Delta\omega_n}{dt} = \Delta P_{m,n} - \Delta P_{e,n} + \Delta p_{o,n} - D_n\Delta\omega_n, \quad (1)$$

where "Δ" stands for the incremental operator, $H_{g,n}$ is the inertia constant, D_n is the damping factor, ω_n is the angular frequency, $P_{m,n}$ is the mechanical power of the equivalent turbine, $P_{e,n}$ is the electrical power demanded by the local load and p_o is the power injected by the n-terminal into the n equivalent generator. The mechanical power ($P_{m,n}$) supplied by the turbine is controlled by using a speed governor that has modelled as a first-order low-pass filter [3]. The transfer function of the turbine and the speed governor can be written as:

$$\Delta P_{m,n} = \Delta P^*_n + R_n/(T_{a,n}s + 1)\cdot(\Delta\omega^*_n - \Delta\omega_n), \quad (2)$$

where R_n is the frequency droop coefficient, $T_{a,n}$ is a time constant that models the transient response of the turbine and the speed governor [17], and P^*_n and ω^*_n are the active power and the angular frequency set points of the n-generator, respectively. For the sake of simplicity, the incremental operator "Δ" will be omitted in the rest of the paper.

C. DC-link Modelling

The energy stored in the dc-link can be modelled by using the following dynamic equation [18]:

$$\underbrace{\frac{C'_{dc}}{2}}_{2H_{dc}}\frac{dv^2_{dc}}{dt} = -\sum_{i=1}^{N_t} p_{dc,i}, \quad (3)$$

where N_t is the number of terminals of the MTDC grid, $p_{dc,i}$ is the instantaneous active power taken from the dc-link by the i-VSC, and H_{dc} is the equivalent inertia constant of the dc link. For control purposes, power losses and energy stored in filters are commonly neglected. Under these considerations, the active power delivered to ac grids is similar to the active power taken from the dc-link [18]. Therefore:

$$2H_{dc}\frac{dv^2_{dc}}{dt} = -\sum_{i=1}^{N_t} p_{o,i}, \quad (4)$$

where $p_{o,i}$ is the instantaneous active power delivered to the i-generator by the i-VSC.

This is the accepted version of an article published in 2020 IEEE Energy Conversion Congress and Exposition - ECCE
http://dx.doi.org/10.1109/ECCE44975.2020.9235831

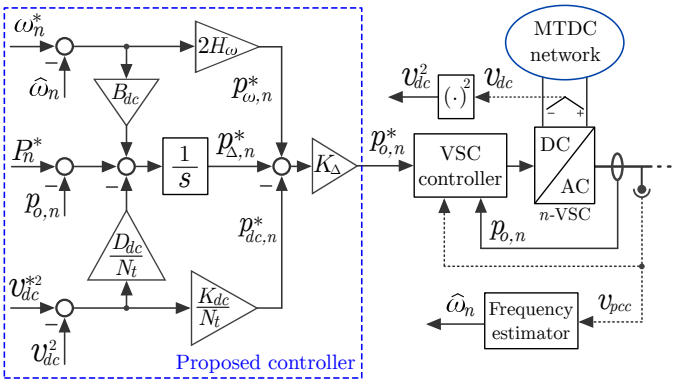

Fig. 2. Block diagram of the proposed controller for the n-VSC.

III. VSC Controller for MTDC Systems

A. Proposed Control System

Fig. 2 shows the block diagram of the proposed controller. The active power delivered by each terminal to its respective ac grid (p_o) can be controlled in order to provide an effect equivalent to an electro-mechanical coupling between the ac networks. Also, a fast regulation of the dc voltage is required. With this aim, the active power reference of the n-VSC controller (p_o^*) is divided into three terms:

$$p_{o,n}^* = K_\Delta \cdot (p_{\Delta,n}^* - p_{dc,n}^* + p_{\omega,n}^*). \tag{5}$$

The term $p_{dc,n}^*$ is used to regulate the dc voltage, the term $p_{\omega,n}^*$ is used to provide inertial support to ac grids, and $p_{\Delta,n}^*$ includes the net active power transfer between ac grids and provides the aforementioned equivalent friction.

A proportional controller is applied over the dc-link voltage error in order to calculate $p_{dc,n}^*$. This is equivalent to a dc droop. Therefore:

$$p_{dc,n}^* = (K_{dc}/N_t)(v_{dc}^{*2} - v_{dc}^2), \tag{6}$$

where v_{dc} is the dc-link voltage and v_{dc}^* is its reference. The controller parameters are defined at the end of this subsection.

Another proportional controller is applied over the ac-frequency error in order to calculate $p_{\omega,n}^*$. This term is used to share frequency deviation information among the MTDC terminals:

$$p_{\omega,n}^* = 2H_{\omega,n}(\omega_n^* - \hat{\omega}_n), \tag{7}$$

where ω_n^* is the frequency reference, and $\hat{\omega}_n$ is the estimated frequency of the n ac grid.

The remaining term is $p_{\Delta,n}^*$, and it used to provide POD features to the controller and to control the net power transfer between ac grids:

$$p_{\Delta,n}^* = \int (P_n^* - p_{o,n} + \underbrace{B_{\omega,n}(\omega_n^* - \hat{\omega}_n)}_{\text{POD controller}} - \frac{D_{dc}}{N_t}(v_{dc}^{*2} - v_{dc}^2)), \tag{8}$$

where P_n^* is the active power reference and $p_{o,n}$ is the active power injected to the ac grid. Fig. 2 shows a block diagram of the proposed controller, which has five parameters:

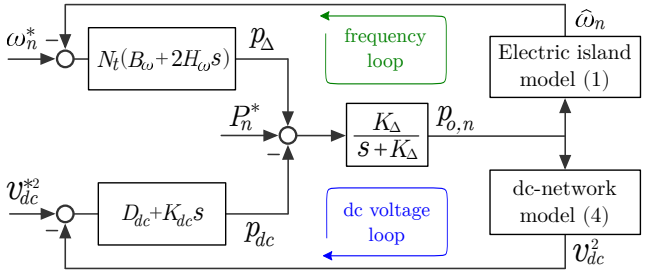

Fig. 3. Equivalent block diagram of the proposed controller for the n-VSC.

1) K_Δ is used to guarantee an adequate transient response the active power controller.
2) $B_{\omega,n}$ is used to provide additional damping to the islanded networks.
3) H_ω is used to share inertia between the islanded networks.
4) K_{dc} and D_{dc} are used to shape the transient response of the dc-voltage controller.

The equivalent electro-mechanical effect of the proposed controller is explained in the following section.

B. Simplified Representation of the Controller

Fig. 3 shows the equivalent block diagram of one VSC with the proposed controller. This block diagram has been obtained by manipulating the one shown in Fig. 2. First, it is assumed that inner controllers dynamics are faster than that of the proposed controller. Therefore, the dynamics of internals controllers are neglected and $p_{o,n}^* \approx p_{o,n}$. Second, the integral action applied over $p_{\Delta,n}^*$ is translated to the command power $(p_{o,n})$. Therefore, derivative actions must be added to the branches of $p_{dc,n}^*$ and $p_{\omega,n}^*$. This modification does not affect the dynamic performance of the controller, but it is best suited for the controller implementation.

The dynamic equations of the active power delivered by the n-VSC to its respective ac grid can written in the Laplace domain as:

$$p_{o,n}(s) = \frac{K_\Delta}{s + K_\Delta}(P_n^* + C_\omega(s)(\omega_n^* - \hat{\omega}_n) - \frac{C_{dc}(s)}{N_t}(v_{dc}^{*2} - v_{dc}^2)), \tag{9}$$

with

$$C_\omega = B_{\omega,n} + H_{\omega,n}s, \tag{10}$$

$$C_{dc} = D_{dc} + K_{dc}s, \tag{11}$$

where $C_\omega(s)$ is the ac frequency controller and $C_{dc}(s)$ is the voltage controller of the MTDC grid.

The proportional control branches that are used to calculate $p_{dc,n}^*$ and $p_{\omega,n}^*$ have an effect equivalent to proportional-derivative controller, yet without explicit derivative actions. The proposed controller will take advantage property to provide:

1) Fast and shared regulation of the dc voltage.
2) Additional inertial response at the terminals connected to low inertia electric islands.

This is the accepted version of an article published in 2020 IEEE Energy Conversion Congress and Exposition - ECCE
http://dx.doi.org/10.1109/ECCE44975.2020.9235831

If references (ω^*, v_{dc}^{*2} and P^*) are constant, a small-signal version of the power expression (9) can be obtained:

$$\Delta p_{o,n}(s) = \underbrace{\frac{K_\Delta}{s+K_\Delta}}_{C_P(s)} \left(-C_\omega(s)\Delta\hat{\omega}_n + \frac{C_{dc}(s)}{N_t}\Delta v_{dc}^2 \right), \quad (12)$$

where $C_P(s)$ is the active power controller. For the sake of simplicity, the incremental operator "Δ" will be omitted in the rest of the paper.

C. Equivalent Mechanical Effect

If the transient response of active power and dc voltage controllers ($C_P(s)$ and $C_{dc}(s)$, respectively) are significantly faster than those of equivalent generators, the dynamics of these controllers can be neglected for system-level analyses [3]. In this case, the power expression (12) becomes:

$$p_{o,n} = -B_{\omega,n}\hat{\omega}_n - 2H_{\omega,n}\frac{d\hat{\omega}_n}{dt} + \frac{D_{dc}}{N_t}v_{dc}^2. \quad (13)$$

By substituting (13) in (1), the equation of the n-equivalent generator can be written as:

$$\begin{aligned} 2H_{g,n}\frac{d\omega_n}{dt} = P_{m,n} - P_{e,n} - D_n\omega_n - B_{\omega,n}\hat{\omega}_n \\ - 2H_{\omega,n}\frac{d\hat{\omega}_n}{dt} + \frac{D_{dc}}{N_t}v_{dc}^2. \end{aligned} \quad (14)$$

Typically, the dynamics of the MTDC grid are significantly faster compared to the dynamics of the ac grids. This means that the equivalent inertia of the MTDC grid would be significantly smaller than that of the equivalent generators ($H_{dc} \ll H_g$). Therefore, from the perspective of the ac grids, the MTDC grid dynamics can be neglected ($dv_{dc}^2/dt \approx 0$). At the power system level, the power balance equation in (4) becomes:

$$\sum_{i=1}^{N_t} p_{o,i} = 0. \quad (15)$$

By substituting the power expression (13) in (15), the following equation is obtained:

$$D_{dc}v_{dc}^2 = \sum_{i=1}^{N_t} B_{\omega,i}\hat{\omega}_i + \frac{d}{dt}\sum_{i=1}^{N_t} 2H_{\omega,i}\hat{\omega}_i. \quad (16)$$

Also, by substituting the term v_{dc}^2 from (16) in (14), the swing equation of the n-equivalent generator becomes:

$$\begin{aligned} 2H_{g,n}\frac{d\omega_n}{dt} = P_{m,n} - P_{e,n} - D_n\omega_n - B_{\omega,n}\hat{\omega}_n \\ - 2H_{\omega,n}\frac{d\hat{\omega}_n}{dt} + \frac{1}{N_t}\sum_{i=1}^{N_t} B_{\omega,i}\hat{\omega}_i + \frac{1}{N_t}\frac{d}{dt}\sum_{i=1}^{N_t} 2H_{\omega,i}\hat{\omega}_i. \end{aligned} \quad (17)$$

In order to clarify the effect of these additional terms, the swing equation (17) can be reorganised and expressed as follow:

$$2H_G\frac{d}{dt}\begin{bmatrix}\omega_1\\ \omega_2\\ \vdots\\ \omega_n\end{bmatrix} = -D_G\begin{bmatrix}\omega_1\\ \omega_2\\ \vdots\\ \omega_n\end{bmatrix} + \begin{bmatrix}P_{m1}\\ P_{m2}\\ \vdots\\ P_{m,n}\end{bmatrix} - \begin{bmatrix}P_{e1}\\ P_{e2}\\ \vdots\\ P_{e,n}\end{bmatrix} \quad (18)$$

where H_G and D_G are the inertia and damping matrices defined in (19) and (20).

It can be seen that the gain $B_{\omega,n}$ introduces additional friction, which is added to the original friction of each area model (D_n). Meanwhile, $H_{\omega,n}$ introduces additional inertia, which is added to the original inertia constant ($H_{g,n}$). Therefore, these control gains can be used to increase both the friction and inertia of an electric island. As a counterpart, additional friction and inertia are subtracted from other electric islands. For example, in the first column of H_G, a term $(N_t-1)/N_tH_{\omega,1}$ is added to the inertia constant of generator G1. However, at the same time, the same term is subtracted from that of generators G2 and G3. This means that the proposed controller introduces a friction and inertia coupling effect among the systems connected though the MTDC terminals.

IV. Case Study and Analytical Results

This section presents a case study consisting of three ac grids interconnected by an MTDC grid (see Fig. 1), which is used to test the proposed controller. Analytical results are shown in order to evaluate controller performance.

A. Simplified Power System Modelling

The dynamics of the equivalent generators including the action of the MTDC link can be expressed as:

$$2H_G\frac{d}{dt}\begin{bmatrix}\omega_1\\ \omega_2\\ \omega_3\end{bmatrix} = -D_G\begin{bmatrix}\omega_1\\ \omega_2\\ \omega_3\end{bmatrix} + \begin{bmatrix}P_{m1}\\ P_{m2}\\ P_{m3}\end{bmatrix} - \begin{bmatrix}P_{e1}\\ P_{e2}\\ P_{e3}\end{bmatrix}, \quad (19)$$

where

$$H_G = \begin{bmatrix} H_{g1}+\frac{2}{3}H_{\omega1} & -\frac{1}{3}H_{\omega2} & -\frac{1}{3}H_{\omega3} \\ -\frac{1}{3}H_{\omega1} & H_{g2}+\frac{2}{3}H_{\omega2} & -\frac{1}{3}H_{\omega3} \\ -\frac{1}{3}H_{\omega1} & -\frac{1}{3}H_{\omega2} & H_{g3}+\frac{2}{3}H_{\omega3} \end{bmatrix}, \quad (20)$$

$$D_G = \begin{bmatrix} D_1+\frac{2}{3}B_{\omega1} & -\frac{1}{3}B_{\omega2} & -\frac{1}{3}B_{\omega3} \\ -\frac{1}{3}B_{\omega1} & D_2+\frac{2}{3}B_{\omega2} & -\frac{1}{3}B_{\omega3} \\ -\frac{1}{3}B_{\omega1} & -\frac{1}{3}B_{\omega2} & D_3+\frac{2}{3}B_{\omega3} \end{bmatrix}. \quad (21)$$

The transfer functions of the combined turbines and speed governors (2) can be represented as a state-space model and merged together (one for each generator), yielding

$$\begin{aligned} \frac{d}{dt}\begin{bmatrix}P_{t1}\\ P_{t2}\\ P_{t3}\end{bmatrix} &= \begin{bmatrix}-1/T_{a1} & 0 & 0\\ 0 & -1/T_{a2} & 0\\ 0 & 0 & -1/T_{a3}\end{bmatrix}\begin{bmatrix}P_{t1}\\ P_{t2}\\ P_{t3}\end{bmatrix} \\ &\quad - \begin{bmatrix}1/T_{a1} & 0 & 0\\ 0 & 1/T_{a2} & 0\\ 0 & 0 & 1/T_{a3}\end{bmatrix}\begin{bmatrix}\omega^*-\omega_1\\ \omega^*-\omega_2\\ \omega^*-\omega_3\end{bmatrix}, \end{aligned} \quad (22)$$

$$\begin{bmatrix}P_{m1}\\ P_{m2}\\ P_{m3}\end{bmatrix} = \begin{bmatrix}R_1 & 0 & 0\\ 0 & R_2 & 0\\ 0 & 0 & R_3\end{bmatrix}\begin{bmatrix}P_{t1}\\ P_{t2}\\ P_{t3}\end{bmatrix} + \begin{bmatrix}P_1^*\\ P_2^*\\ P_3^*\end{bmatrix}. \quad (23)$$

By merging the state-space models (19), (22) and (23), the simplified power system model can be obtained.

B. Case Study

Table I shows the parameters, damping factor and oscillation frequencies of the equivalent generators. By using

This is the accepted version of an article published in 2020 IEEE Energy Conversion Congress and Exposition - ECCE
http://dx.doi.org/10.1109/ECCE44975.2020.9235831

$$H_G = \begin{bmatrix} H_{g1} + \frac{N_t-1}{N_t} H_{\omega 1} & -\frac{1}{N_t} H_{\omega 2} & \cdots & -\frac{1}{N_t} H_{\omega,n} \\ -\frac{1}{N_t} H_{\omega 1} & H_{g2} + \frac{N_t-1}{N_t} H_{\omega 2} & \cdots & -\frac{1}{N_t} H_{\omega,n} \\ \vdots & & \ddots & \vdots \\ -\frac{1}{N_t} H_{\omega 1} & -\frac{1}{N_t} H_{\omega 2} & \cdots & H_{g,n} + \frac{N_t-1}{N_t} H_{\omega,n} \end{bmatrix}, \tag{19}$$

$$D_G = \begin{bmatrix} D_1 + \frac{N_t-1}{N_t} B_{\omega 1} & -\frac{1}{N_t} B_{\omega 2} & \cdots & -\frac{1}{N_t} B_{\omega,n} \\ -\frac{1}{N_t} B_{\omega 1} & D_2 + \frac{N_t-1}{N_t} B_{\omega 2} & \cdots & -\frac{1}{N_t} B_{\omega 3} \\ \vdots & & \ddots & \vdots \\ -\frac{1}{N_t} B_{\omega 1} & -\frac{1}{N_t} B_{\omega 2} & \cdots & D_3 + \frac{N_t-1}{N_t} B_{\omega,n} \end{bmatrix}, \tag{20}$$

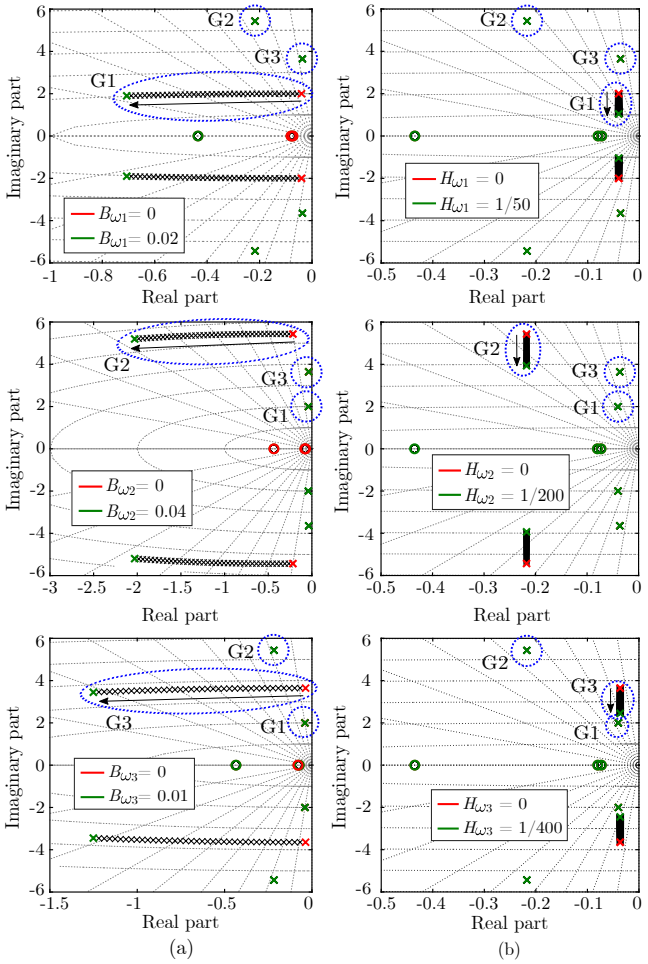

Fig. 4. (a) Pole trajectories of the simplified power system for (a) different damping gain values ($B_{\omega 1}$, $B_{\omega 2}$ and $B_{\omega 3}$), (b) different inertial gain values ($H_{\omega 1}$, $H_{\omega 2}$ and $H_{\omega 3}$).

these parameters, generators G1, G2 and G3 exhibit poorly damped resonances ($\zeta < 0.05$) and oscillation frequencies of $\omega_{os1} = 2$ rad/s, $\omega_{os2} = 5.4$ rad/s and $\omega_{os3} = 3.64$ rad/s, respectively.

C. Analysis of the Additional Damping Effect

In Section III-C, it has been shown that the gains $B_{\omega,n}$ introduce additional damping added to the damping factor of each generator. The impact of the gain B_ω on the local oscillation modes of generators G1, G2 and G3 is analysed in this section. For this analysis, the additional inertia gains were set to zero ($H_\omega = 0$).

Fig. 4(a) shows the trajectories of the closed-loop poles when the damping gain of each terminal ($B_{\omega 1}$, $B_{\omega 2}$ and $B_{\omega 3}$) varied. When $B_\omega = 0$ (red poles), the networks are completely decoupled and the system exhibit three groups of poorly damped poles that correspond to each of the equivalent generators (marked as G1, G2 and G3). The poles show the expected damping and oscillation frequency values. When the damping gains B_ω increase, the poles of the equivalent generators move away from the unstable region, increasing their damping factor.

TABLE I
PARAMETERS OF THE EQUIVALENT GENERATORS

Var.	Value	Var.	Value	Var.	Value
H_1	1/200 pu	H_2	1/271 pu	H_3	1/728 pu
D_1	0	D_2	0	D_3	0
R_1	0.5	R_2	0.5	R_3	0.5
T_1	12.5 s	T_2	2.3 s	T_3	13.7 s
ζ_1	0.02	ζ_2	0.04	ζ_3	0.01
ω_{os1}	2 rad/s	ω_{os2}	5.4 rad/s	ω_{os3}	3.64 rad/s

D. Analysis of the Additional Inertial Effect

In Section III-C, it has been shown that the gains $H_{\omega,n}$ introduce additional inertia added to the inertia constant of each generator. The impact of the gain H_ω on the local oscillation modes of generators G1, G2 and G3 is analysed in this section. For this analysis, the additional damping gains were set to zero ($B_\omega = 0$).

Fig. 4(b) show the trajectories followed by the closed-loop poles when the additional inertia gain of each terminal ($H_{\omega 1}$, $H_{\omega 2}$ and $H_{\omega 3}$) varied. When $H_\omega = 0$ (red poles), the system exhibit the poles of the equivalent generators. When the inertia gains H_ω increase, the poles of the generator move parallel to the imaginary axis, reducing their frequency.

V. Simulation Results

The proposed control scheme and the theoretical developments were validated on a detailed simulation model developed in Matlab/Simulink. The nominal frequency of the ac networks was set to 50 Hz. A fourth-order synchronous machine model was used to emulate the dynamics of the ac power networks. The synchronous machine parameters

This is the accepted version of an article published in 2020 IEEE Energy Conversion Congress and Exposition - ECCE
http://dx.doi.org/10.1109/ECCE44975.2020.9235831

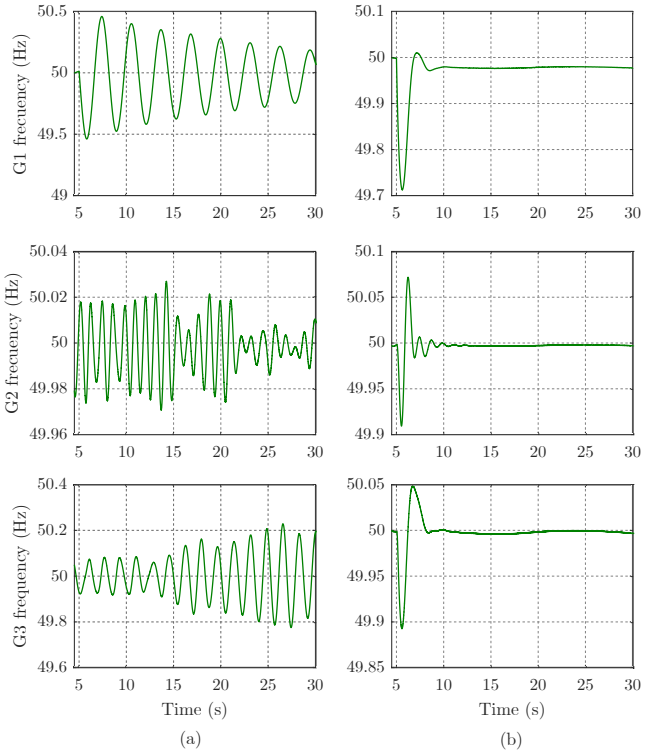

Fig. 5. Simulation results: Transient response of the system when a step change of the load connected to G1 is applied, (a) the virtual coupling is disabled (b) the virtual coupling is enabled.

are shown in Table I. The virtual coupling gains were set to $B_{\omega 1} = 0.0282$, $H_{\omega 1} = 2.28 \cdot 10^{-3}$, $B_{\omega 2} = 0.0461$, $H_{\omega 2} = 4.61 \cdot 10^{-3}$, and $B_{\omega 3} = 0.0166$, $H_{\omega 3} = 1.66 \cdot 10^{-3}$.

Fig. 5(a) shows the transient response of the system when a step change of the load connected to generator G1 was applied and the virtual coupling was disabled. It can be seen that the three ac power networks are decoupled and generator G3 exhibits the damping and natural frequency shown in Table I. Fig. 5(b) shows the transient response of the system when a step change of the load connected to generator G1 was applied and the virtual coupling was enabled. It can be seen that, when the load was connected, the proposed controller introduced an active power exchange between the power networks, which is proportional to the frequency deviation (B_ω) and its derivative (H_ω). This active power exchange introduces the virtual electro-mechanical coupling that damps the frequency oscillations.

VI. Conclusion

In this paper, a controller for multi-terminal VSC-HVDC interconnections that provides virtual mechanical coupling between asynchronous ac networks has been proposed. It has been shown that this mechanical effect is equivalent to the mechanical friction of the coupling between rotating masses of equivalent generators. Moreover, it introduces an inertial sharing effect between the ac networks. The controller has been parametrized so that the equivalent virtual frictions and the inertia sharing effect are represented by independent gains of the controller. The performance of the controller was validated in simulation, and results showed that lightly-damped frequency oscillations can be effectively damped by using the proposed virtual coupling.

References

[1] J. Renedo, A. García-Cerrada, L. Rouco, and L. Sigrist, "Coordinated control in vsc-hvdc multi-terminal systems to improve transient stability: The impact of communication latency," *Energies*, vol. 12, no. 19, 2019. [Online]. Available: https://www.mdpi.com/1996-1073/12/19/3638

[2] D. V. Hertem and M. Ghandhari, "Multi-terminal vsc hvdc for the european supergrid: Obstacles," *Renewable and Sustainable Energy Reviews*, vol. 14, no. 9, pp. 3156 – 3163, 2010. [Online]. Available: http://www.sciencedirect.com/science/article/pii/S1364032110002480

[3] P. Kundur, N. Balu, and M. Lauby, *Power System Stability and Control*, ser. Discussion Paper Series. McGraw-Hill Education, 1994. [Online]. Available: https://books.google.es/books?id=2cbvyf8Ly4AC

[4] J. P. Sucena-Paiva and L. L. Freris, "Stability of a d.c. transmission link between strong a.c. systems," *Proceedings of the Institution of Electrical Engineers*, vol. 120, no. 10, pp. 1233–1242, October 1973.

[5] M. A. Hannan, I. Hussin, P. J. Ker, M. M. Hoque, M. S. Hossain Lipu, A. Hussain, M. S. A. Rahman, C. W. M. Faizal, and F. Blaabjerg, "Advanced control strategies of vsc based hvdc transmission system: Issues and potential recommendations," *IEEE Access*, vol. 6, pp. 78 352–78 369, 2018.

[6] R. Shah, J. Sánchez, R. Preece, and M. Barnes, "Stability and control of mixed ac-dc systems with vsc-hvdc: A review," *IET Generation, Transmission & Distribution*, January 2018.

[7] L. Huang, H. Xin, W. Dong, and F. Dorfler, "Impacts of grid structure on pll-synchronization stability of converter-integrated power systems," 2019.

[8] L. Huang, H. Xin, H. Yang, Z. Wang, and H. Xie, "Interconnecting very weak ac systems by multiterminal vsc-hvdc links with a unified virtual synchronous control," *IEEE Journal of Emerging and Selected Topics in Power Electronics*, vol. 6, no. 3, pp. 1041–1053, Sep. 2018.

[9] Y. Cao, W. Wang, Y. Li, Y. Tan, C. Chen, L. He, U. Hger, and C. Rehtanz, "A virtual synchronous generator control strategy for vsc-mtdc systems," *IEEE Tran Energy Conversion*, vol. 33, no. 2, pp. 750–761, June 2018.

[10] R. Aouini, B. Marinescu, K. Ben Kilani, and M. Elleuch, "Synchronverter-based emulation and control of hvdc transmission," *IEEE Tran. on Power Systems*, vol. 31, no. 1, pp. 278–286, Jan 2016.

[11] L. Zeni, R. Eriksson, S. Goumalatsos, M. Altin, P. Srensen, A. Hansen, P. Kjr, and B. Hesselbk, "Power oscillation damping from vschvdc connected offshore wind power plants," *IEEE Tran Power Del*, vol. 31, no. 2, pp. 829–838, April 2016.

[12] Y. Shen, W. Yao, J. Wen, H. He, and W. Chen, "Adaptive supplementary damping control of vsc-hvdc for interarea oscillation using grhdp," *IEEE Tran Power Systems*, vol. 33, no. 2, pp. 1777–1789, March 2018.

[13] R. Preece, J. V. Milanovi, A. M. Almutairi, and O. Marjanovic, "Damping of inter-area oscillations in mixed ac/dc networks using wams based supplementary controller," *IEEE Tran Power Systems*, vol. 28, no. 2, pp. 1160–1169, May 2013.

[14] B. Pierre, R. Elliott, D. Schoenwald, J. Neely, R. Byrne, D. Trudnowski, and J. Colwell, "Supervisory system for a wide area damping controller using pdci modulation and real-time pmu feedback," in *2016 IEEE Power and Energy Society General Meeting*, 2016, pp. 1–5.

[15] Y. Han, H. Li, P. Shen, E. A. A. Coelho, and J. M. Guerrero, "Review of active and reactive power sharing strategies in hierarchical controlled microgrids," *IEEE Tran Power Elec*, vol. 32, no. 3, pp. 2427–2451, March 2017.

[16] A. Rodríguez-Cabero, J. Roldán-Pérez, M. Prodanovic, J. A. Suul, and S. DArco, "Coupling of ac grids via vsc-hvdc interconnections for oscillation damping based on differential and common power control," *IEEE Tran Power Elec*, vol. 35, no. 6, pp. 6548–6558, 2020.

[17] H. Bevrani, B. François, and T. Ise, *Microgrid Dynamics and Control*. Wiley, 2017.

[18] A. Rodríguez-Cabero, M. Prodanovic, and J. Roldán-Pérez, "Full-state feedback control of back-to-back converters based on differential and common power concepts," *IEEE Tran Ind Elec*, pp. 1–1, 2018.

This is the accepted version of an article published in 2020 IEEE Energy Conversion Congress and Exposition - ECCE
http://dx.doi.org/10.1109/ECCE44975.2020.9235831